JOURNAL OF Applied Polymer SCIENCE

Electrospinning preparation, characterization, and enhanced photocatalytic activity of an Silicotungstic acid ($H_4SiW_{12}O_{40}$)/poly(vinyl alcohol)/poly(methyl methacrylate) composite nanofiber membrane

Tingting Li,[1] Zhiming Zhang,[1] Wei Li,[1] Ce Liu,[2] Haoyu Zhou,[1] Libao An[3]

[1]College of Material Science and Engineering, North China University of Science and Technology, Hebei Provincial Key Laboratory of Inorganic Nonmetallic Materials, Tangshan 063009, China

[2]College of Chemical Engineering, North China University of Science and Technology, Tangshan 063009, China

[3]College of Mechanical Engineering, North China University of Science and Technology, Tangshan 063009, China

Correspondence to: Z. Zhang (E-mail: zhangzhiming1942@163.com) and L. An (E-mail: lan@ncst.edu.cn)

ABSTRACT: Silicotungstic acid ($H_4SiW_{12}O_{40}$)/poly(vinyl alcohol) (PVA)/poly(methyl methacrylate) (PMMA) composite nanofiber membranes were prepared by an electrospinning technique. A PMMA emulsion was mixed with PVA and $H_4SiW_{12}O_{40}$ evenly in water (electrospinning solvent). The configuration and elemental composition of the membranes were characterized by scanning electron microscopy, Fourier transform infrared spectroscopy, and X-ray photoelectron spectroscopy. The results indicate that $H_4SiW_{12}O_{40}$ with an intact Keggin structure existed in the composite membrane. The as-prepared $H_4SiW_{12}O_{40}$/PVA/PMMA membranes exhibited enhanced photocatalytic efficiency (>84%) in the degradation of methyl orange (MO); it outperformed $H_4SiW_{12}O_{40}$ powder (4.6%) and the $H_4SiW_{12}O_{40}$/PVA nanofiber membrane (75.2%) under UV irradiation. More importantly, the $H_4SiW_{12}O_{40}$/PVA/PMMA membranes could be easily separated from the aqueous MO solution, and the photocatalytic efficiency of the membranes decreased inappreciably after three photocatalytic cycles. This may have been due to the enhanced water tolerance of the membranes and the stability of $H_4SiW_{12}O_{40}$ in the membranes. The photocatalytic process was driven by the reductive pathway with a much faster degradation rate because of the presence of PVA. © 2015 Wiley Periodicals, Inc. J. Appl. Polym. Sci. **2016**, *133*, 43193.

KEYWORDS: catalysts; electrospinning; membranes; photochemistry; recycling

Received 1 August 2015; accepted 7 November 2015

DOI: 10.1002/app.43193

INTRODUCTION

Polyoxometalates (POMs) are well-defined, early transition metal–oxygen clusters with unique structural characteristics. POMs can behave as photocatalysts by the photoexcitation of the oxygen-to-metal charge-transfer bands to separate the electron-hole pair used for reductive and oxidative reactions with surrounding molecules.[1] They have some advantages, including optical stability, adjustable oxidizability, a more stable chemical structure, nontoxicity, and low cost; this results in their successful use in the photodegradation of various organic pollutants, especially in the decomposition of organic dyes.[2–4] However, the high water solubility of POMs, which impedes the ready recovery and reuse of the photocatalysts, is still a challenge.[5] For the purpose of practical applications, it is desirable to develop a heterogeneous photocatalytic system through the combination of POMs with supporting materials to make them more recoverable. Therefore, considerable interest has been focused on the coupling of POMs with many supports, such as silica, activated carbons, TiO_2, mesoporous molecular sieves, and polymeric membranes.[6–10] From the standpoint of the separation and recovery of catalysts in practical wastewater treatment, POM-containing films are more predominant compared with powdered POM materials because no separation process is needed for the films. To the best of our knowledge, there have been some studies on the photocatalytic properties of POM-containing composite films prepared by the layer-by-layer self-assembly method[11] and sol–gel technique.[2] However, few reports have been made on the photocatalytic application of POM-containing composite films prepared by electrospinning.

The electrospinning technique is a simple, versatile, and effective method for preparing polymers, polymer/inorganic hybrids, and inorganic nanofibers.[12,13] Nanofiber membranes have many remarkable characteristics, including fine diameters ranging from submicrometers to several nanometers,[14,15] large specific surface areas, high porosities, and high permeabilities.[16] Hence, electrospun nanofiber membranes may be promising supports

for the immobilization of photocatalysts. Briefly, the qualification of electrospun nanofiber membranes as excellent supports is attributed to (1) their easier separation and reuse because of their nonwoven mesh forms and (2) the high-level exposure of the photocatalysts, which is due to the large surface areas of the one-dimensional nanofibers.[17] It was reported that Brunauer–emmett–teller specific surface areas of POMs were lower than 10 m^2/g,[18] and the specific surface areas of the supported POMs could be largely increased compared with those of the parent POMs.[19] Zhou[20] used Silicotungstic acid ($H_4SiW_{12}O_{40}$) as a template and prepared Ag/poly(vinyl alcohol) (PVA)/SiW_{12} tricomponent nanohybirds with electrospinning and photoreduction methods. The photocatalytic activity of the nanohybirds was signally improved because of the synergistic effect of the three components.

In this study, PVA/poly(methyl methacrylate) (PMMA) composite nanofiber membranes were prepared by electrospinning as the supporter of $H_4SiW_{12}O_{40}$. PVA was chosen primarily for two reasons:

1. PVA can interact with $H_4SiW_{12}O_{40}$ through hydrogen bonds. This would inhibit the leakage of $H_4SiW_{12}O_{40}$ from the support during the photocatalytic process
2. PVA is a polymer in common use with a high mechanical strength and good spinnability.

Nevertheless, as a water-soluble polymer, the structure and porosity of electrospun PVA nanofibers disappear when the membrane is immersed in water for just a few minutes. It is impractical for its application as a support in an aqueous environment. Crosslinking is a widely used and effective method for making PVA nanofibers insoluble, but it would result in the alteration of the chemical properties of PVA. In view of this, the composite nanofiber membranes were prepared by the blending of PVA, PMMA, and $H_4SiW_{12}O_{40}$ in specific ratios. The water tolerance of PMMA could inhibit the osmosis of the aqueous solution into the composite nanofibers and improve the stability of the composite membranes in water. To mix PMMA with PVA and $H_4SiW_{12}O_{40}$ evenly in water (the electrospinning solvent), PMMA was added in the form of an emulsion. To the best of our knowledge, this is the first report on the preparation of $H_4SiW_{12}O_{40}$/PVA/PMMA composite nanofiber membranes and their photocatalytic properties and mechanism. This information will be useful for further study on the design of nanofiber membranes for photocatalytic applications in the treatment of practical waste effluents.

EXPERIMENTAL

Materials

$H_4SiW_{12}O_{40}$, sodium dodecyl benzene sulfonate, potassium persulfate ($K_2S_2O_8$), and perchloric acid ($HClO_4$) which were analytical-reagent grade, were supplied by Sinopharm Chemical Reagent Co., Ltd. PVA (weight-average molecular weight = 75,000) was also purchased from Sinopharm Chemical Reagent Co., Ltd. Methyl methacrylate (MMA), alkylphenol ethoxylates(OP-10) emulsifier, and methyl orange (MO) were purchased from Aladdin Industrial Corp. All of the aqueous solutions were prepared by deionized water.

Preparation of the $H_4SiW_{12}O_{40}$/PVA/PMMA Composite Nanofiber Membrane

MMA emulsion polymerization was carried out in a 250-mL flask equipped with a motor agitator, a thermometer, a nitrogen inlet, and a reflux condenser. A mixture of MMA and H_2O (mass ratio = 3:10), alkylphenol ethoxylates (OP-10), and PVA was placed in the reactor and stirred at 80°C until an emulsion was formed before polymerization. A $K_2S_2O_8$ solution ($K_2S_2O_8$/MMA weight ratio = 1:100) was fed into the reactor when the content in the reactor reached the designed polymerization temperature. The polymerization proceeded under a nitrogen atmosphere.

The electrospinning solution was prepared by the dissolution of 1.5 g of PVA in 15 mL of deionized water with stirring until PVA was completely dissolved at 80°C; then, the PMMA emulsion (2.5, 5, and 7.5 mL, respectively) was added to the previous solution with stirring for an additional 1 h at 80°C. After it cooled to room temperature, 1.0 g of $H_4SiW_{12}O_{40}$ was added to the mixed solution. The as-prepared electrospinning solution was added to a 5-mL glass syringe with a needle tip (0.5 mm in diameter). The flow rate of the solution was 0.5 mL/h; this was controlled by a microsyringe pump. The used voltage was 20 kV, and the collection distance between the needle tip and aluminum foil was 15 cm.

Photocatalytic Activity Testing

The photocatalytic activity of the composite nanofiber membranes was evaluated for the decomposition of harmful aqueous MO. A 300-W, high-pressure mercury lamp with a double-walled quartz glass tube (for water cooling) was suspended vertically (the distance between the quartz glass reactor and the lamp was 10 cm). The photodegradation of MO was carried out at atmospheric pressure and room temperature. In a typical experiment, 50 mL of an MO aqueous solution (10 mg/L; the pH was adjusted to 1.0 with $HClO_4$) was placed in the reactor, and the composite nanofiber membrane was immersed in the solution. Before the irradiation, the reactor was stirred in the dark for 30 min to establish an adsorption–desorption equilibrium between the organic molecules and the catalyst surface. Decreases in the concentrations of MO were analyzed with an ultraviolet–visible (UV–vis) spectrophotometer at a wavelength of 510 nm. At given intervals of illumination, samples (5 mL) of the reaction solution were taken out and analyzed.

Instrumentation and Characterization

The inject rate of the electrospinning solution was controlled by a 78-9100C syringe pump (Cole Palmer Instrument Co.). The nozzle was connected to a high-voltage regulated direct-current power supply (DW-P503-4ACCD, Tianjin Dongwen High Voltage Power Supply Plant). Fourier transform infrared (FTIR) spectra were recorded with a Nicolet 380 spectrometer and were obtained at a resolution of 4 cm^{-1}. The micrographs of the composite nanofiber membranes were analyzed with a Hitachi S-4800 field emission scanning electron microscope. X-ray photoelectron spectroscopy (XPS) measurement was carried out with a ESCALAB 250Xi spectrometer with nonmonochromatized Al Kα X-ray radiation [UV photon energy ($h\nu$) = 1486.6 eV] and a power of 150 W (10 mA × 15 kV). The

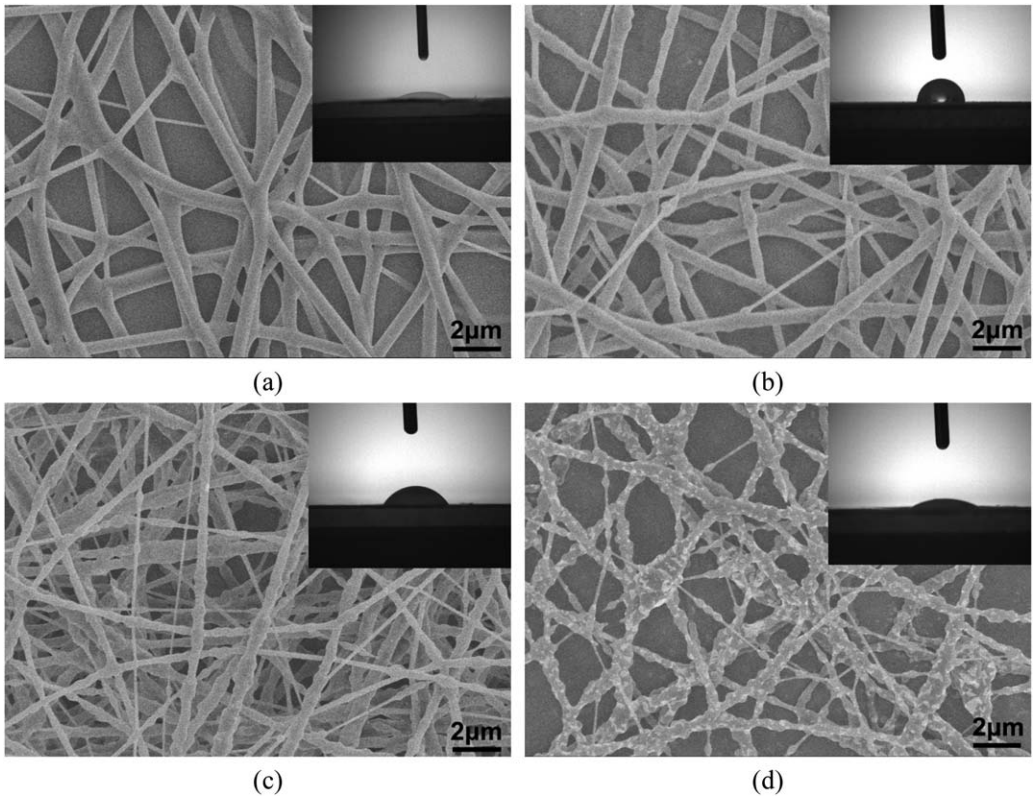

Figure 1. SEM images of the (a) $H_4SiW_{12}O_{40}$/PMMA and (b–d) $H_4SiW_{12}O_{40}$/PVA/PMMA composite nanofibers with different mass ratios of PMMA to PVA (1:2, 1:1, and 2:1, respectively). The insets present the contact angles of the composite nanofiber membranes.

concentrations of the MO solutions were measured by a Specord S-600 UV–vis spectrophotometer (Analytik Jena AG Co.) over the wavelength range 200–800 nm.

RESULTS AND DISCUSSION

Characterization of the Composite Nanofiber Membranes

The morphologies of the as-prepared nanofibers were characterized by field emission scanning electron microscopy (Figure 1). Figure 1(a) shows a typical scanning electron microscopy (SEM) image of the $H_4SiW_{12}O_{40}$/PVA composite nanofibers. We observed that these randomly oriented fibers had relatively smooth surfaces, and the diameters ranged from 400 to 620 nm. Figure 1(b–d) shows the morphologies of the $H_4SiW_{12}O_{40}$/PVA/PMMA fibers with different mass ratios of PMMA to PVA. As the mass ratio increased, a beaded structure became obvious, and the fibers surface became rough. As is apparent from Figure 1(d), beads were predominantly deposited, and the nanofibers appeared to consist of linked particles. As shown in the inset images, the contact angle of the $H_4SiW_{12}O_{40}$/PVA composite nanofiber membrane was 27.4°; this was due to the high hydrophilicity of PVA. The contact angle for the $H_4SiW_{12}O_{40}$/PVA/PMMA composite nanofiber membrane was higher; this was due to the hydrophobicity of PMMA. The addition of PMMA could have created hydrogen bonds between PMMA and PVA and reduced the number of —OH groups exposed on the surface of the composite nanofiber membranes.[21,22] However, the contact angle decreased when the mass ratio of PMMA to PVA increased; this was primarily because of the enhanced hydrophilicity of the membrane surface induced by the surface roughness.[23]

The FTIR spectra of PVA, PMMA, $H_4SiW_{12}O_{40}$, and the $H_4SiW_{12}O_{40}$/PVA/PMMA composite nanofiber membrane are shown in Figure 2. For PVA, the broad peak at 3265–3472 cm^{-1} corresponded to the stretching of O—H bonds. The peak at 2945 cm^{-1} was due to the C—H stretching of alkyl groups, and the peak at 1128 cm^{-1} was attributed to the stretching of C—O bonds. For PMMA, the peak at 1727 cm^{-1} was typical of C=O stretching in the ester group. For $H_4SiW_{12}O_{40}$, the characteristic absorption peaks of the Keggin unit at 1017, 980, 922, and 792 cm^{-1} were attributed to ν_{as}(Si—O_a), ν_{as}(W=O_d), ν_{as}(W—O_b—W) and ν_{as}(W—O_c—W), respectively.[20] The FTIR spectrum of the $H_4SiW_{12}O_{40}$/PVA/PMMA composite nanofiber membrane had nearly all of the key features of PVA, PMMA, and $H_4SiW_{12}O_{40}$ with minor shifts of some peaks. It was obvious that the composite sample displayed four discernible peaks between 790 and 1100 cm^{-1}; this agreed well with the Keggin unit and indicated that the Keggin structure of $H_4SiW_{12}O_{40}$ remained intact in the $H_4SiW_{12}O_{40}$/PVA/PMMA composite nanofiber membrane.[24] Shifts were observed in the peaks corresponding to ν_{as}(W=O_d) from 980 to 971 cm^{-1} and ν_{as}(W—O_c—W) from 792 to 799 cm^{-1}. The peak at 3265–3472 cm^{-1}, which was related to O—H, shifted to a lower wave number, and the intensity of the broad peak weakened significantly. All of the changes indicated that there may have been weak interactions, such as hydrogen bonds, between PVA and $H_4SiW_{12}O_{40}$; this was propitious for the

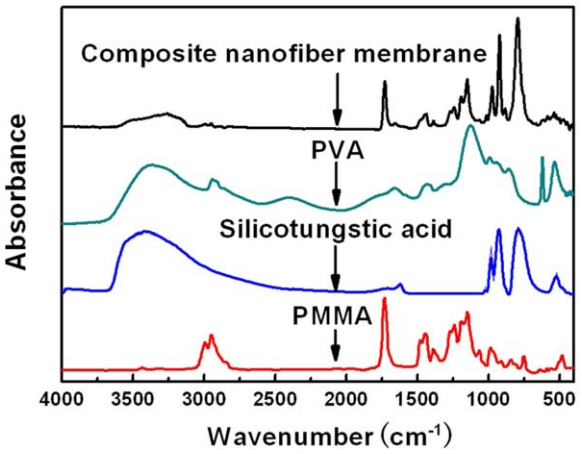

Figure 2. FTIR spectra of the PMMA, $H_4SiW_{12}O_{40}$, PVA, and $H_4SiW_{12}O_{40}$/PVA/PMMA composite nanofiber membranes. [Color figure can be viewed in the online issue, which is available at wileyonlinelibrary.com.]

immobilization of $H_4SiW_{12}O_{40}$ and ensured little leakage from the support during the photocatalytic process.

To further investigate the surface chemical composition and the valence state of W in the composite nanofiber membrane, XPS measurement was carried out. Figure 3(a) shows the survey spectrum of the $H_4SiW_{12}O_{40}$/PVA/PMMA composite nanofiber membrane; it indicated the presence of W, Si, C, O, S, and Na from the reference. For the W 4f XPS spectrum, as shown in Figure 3(b), two different chemical states of W were observed. A spin-orbit doublet with a binding energy for the W $4f_{7/2}$ core level of 35.8 eV accounted for approximately 91.0% of the total spectral area. This value is typical of the presence of W(VI) and was ascribed to $H_4SiW_{12}O_{40}$ in the composite membrane. A second doublet at 34.5 eV ($4f_{7/2}$ component) accounted for the remaining area. According to the previous literature, this value may indicate the existence of perturbed tungstate environments corresponding to tungsten atoms in the terminal W═O bonds that directly coordinate to the support.[25] The O1s spectrum of the sample was deconvoluted into two components [Figure 3(c)]. The peak at 530.7 eV was attributed to the lattice oxygen in the Keggin structure (W—O—W); this was in good agreement with the results reported elsewhere.[26] The component with a higher binding energy at 532.4 eV was assigned to C—O and arose from PVA and PMMA. The C1s spectrum of the composite nanofiber membrane contained three distinct contributions, which were due to the presence of C—C (284.8 eV), C—O—C (286.1 eV), and O—C═O (288.5 eV) [Figure 3(d)].

Photocatalytic Properties

Photocatalytic Activity. The photocatalytic activities of the $H_4SiW_{12}O_{40}$/PVA/PMMA composite nanofiber membranes were tested by degradation of aqueous MO under UV irradiation.

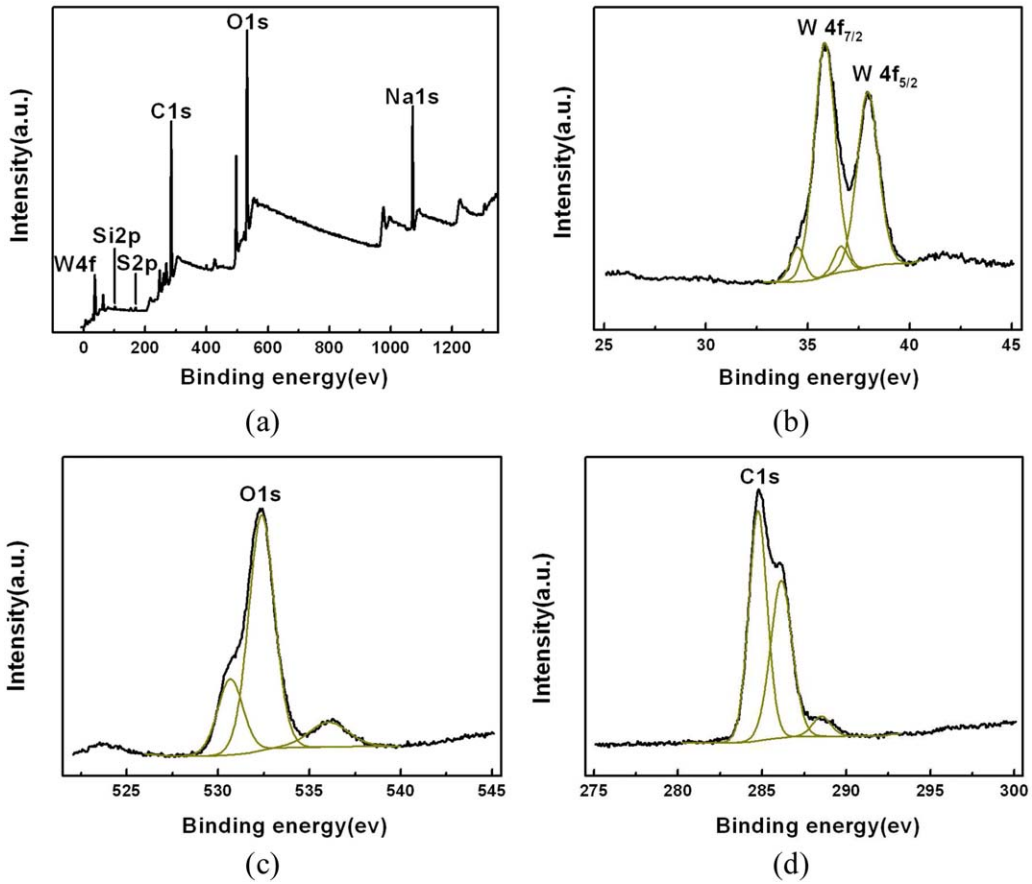

Figure 3. XPS spectra of the $H_4SiW_{12}O_{40}$/PVA/PMMA composite nanofiber membranes: (a) wide-scan and (b) narrow-scan W outer nuclear electronic layers (4f) spectra, (c) O1s spectra, and (d) C1s spectra. [Color figure can be viewed in the online issue, which is available at wileyonlinelibrary.com.]

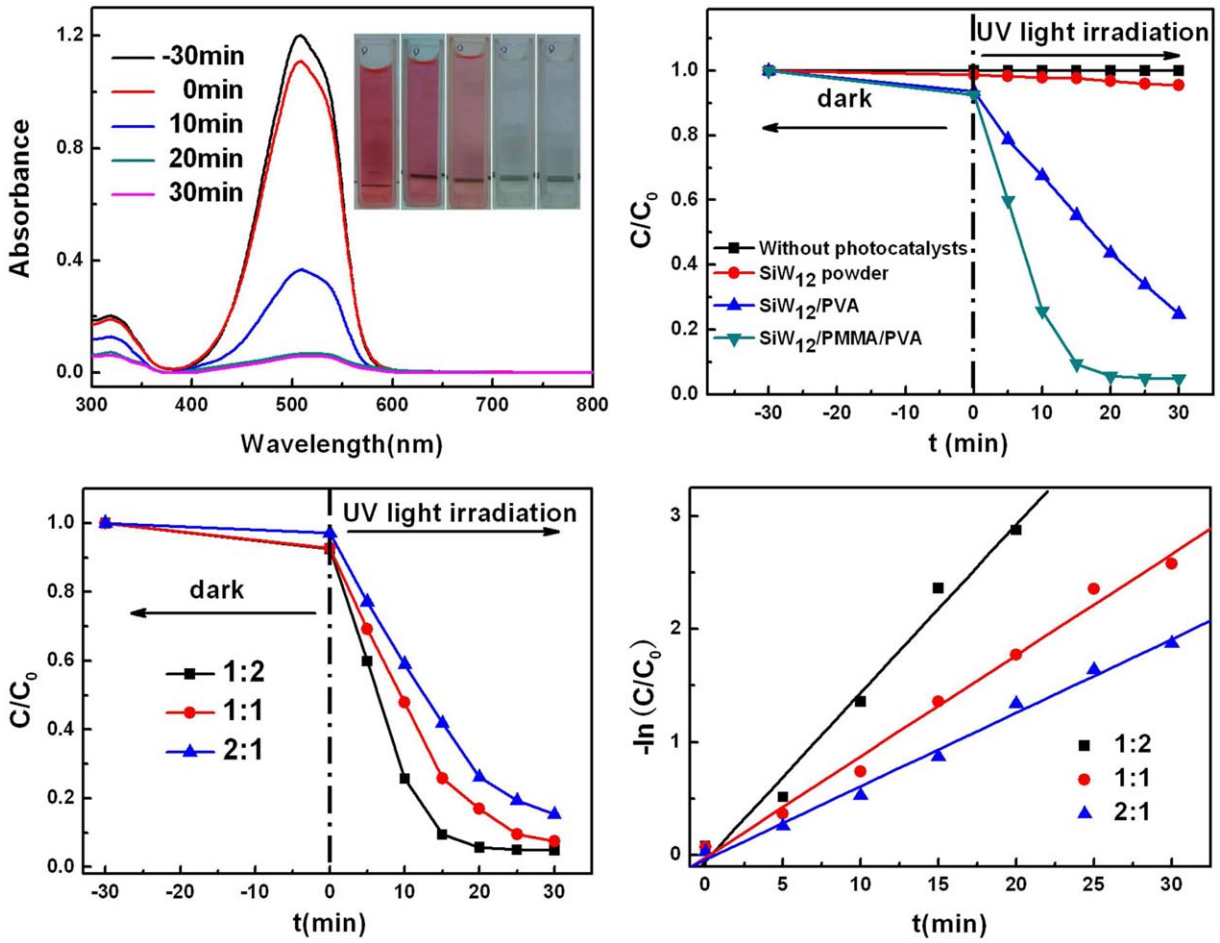

Figure 4. (a) UV–vis absorption spectra variation of MO versus the photoreaction time for the composite nanofiber membrane (mass ratio of PMMA to PVA = 1:2), (b) photodegradation of MO with different catalysts against the irradiation time under UV light, (c) photodegradation of MO against the irradiation time, and (d) pseudo-first-order kinetic treatment of the composite nanofiber membranes with different mass ratios of PMMA to PVA. [Color figure can be viewed in the online issue, which is available at wileyonlinelibrary.com.]

Figure 4(a) shows the absorption spectra variation of MO versus the irradiation time on the composite nanofiber membranes, in which the mass ratio of PMMA to PVA was 1:2. The major absorption peaks of MO around 510 nm decreased rapidly, whereas the color of the aqueous MO solution changed from red to nearly colorless after 30 min; this indicated a nearly complete degradation of MO.

As a comparison, the photocatalytic performances of the $H_4SiW_{12}O_{40}$ powder (0.05 g) and $H_4SiW_{12}O_{40}$/PVA composite nanofiber membrane were also evaluated. There was 0.05 g of $H_4SiW_{12}O_{40}$ in every composite nanofiber membrane. As shown in Figure 4(b), in the absence of a photocatalyst with UV irradiation, no obvious degradation of MO was observed. In the presence of the photocatalysts, the absorbance of the MO solution decreased with increasing irradiation time. After UV-light irradiation for 30 min, the degradation efficiencies of MO were about 4.6, 75.2, and 95.1% for the $H_4SiW_{12}O_{40}$ powder, $H_4SiW_{12}O_{40}$/PVA composite nanofiber membrane, and $H_4SiW_{12}O_{40}$/PVA/PMMA composite nanofiber membrane, respectively. Obviously, the $H_4SiW_{12}O_{40}$/PVA/PMMA composite nanofiber membrane exhibited a much higher photocatalytic activity than the $H_4SiW_{12}O_{40}$ powder and $H_4SiW_{12}O_{40}$/PVA composite nanofiber membrane under the same conditions. The primary reason may have been that PMMA with a high hydrophobicity inhibited the osmosis of the aqueous solution into the composite nanofibers and improved the stability of the composite nanofiber membrane in water. In addition, compared with that of the $H_4SiW_{12}O_{40}$ powder, the high specific surface area of the nanofiber membrane and the completely different photocatalytic mechanism, due to the presence of PVA, resulted in the enhancement of the degradation rate of MO (see later discussion).

For further investigation, $H_4SiW_{12}O_{40}$/PVA/PMMA composite nanofiber membranes with different mass ratios of PMMA to PVA were evaluated. Their photocatalytic activities are shown in Figure 4(c). Degradations of 95.1, 92.4, and 84.7% of MO were observed after 30 min of irradiation for the composite nanofiber membranes in which the PMMA/PVA ratios were 1:2, 1:1, and 2:1, respectively. Among the three samples, the composite nanofiber membrane in which the PMMA/PVA ratio was 1:2 displayed the best photocatalytic activity. The degradation of MO was more than 90% after only 15 min of irradiation for

Table I. Comparison of the Photocatalytic Efficiencies of Different Catalysts for the Degradation of MO

Catalyst	Catalytic conditions	MO degradation (%)	Reference
TiO_2 film	$[TiO_2] = 120$ ppm, $[MO] = 1.9 \times 10^{-5}$ *M*, and initial pH of 9.2 after 1 h of illumination	50	29
Ag/TiO_2 film	$[TiO_2] = 120$ ppm, $[MO] = 1.9 \times 10^{-5}$ *M*, $[AgNO_3] = 10^{-3}$ *M*, and initial pH of 9.2 after 1 h of illumination	90	29
Sulfate-modified titanium dioxide (SO_4^{2-}/TiO_2 catalyst)	[Catalyst] = 1.0 g/L, $[SO_4^{2-}] = 2.5$ wt %, [MO] = 150 mg/L, and 4 h	61	30
Anodized TiO_2 nanotube array	TiO_2 photoanode, [MO] = 40 m*M*, electrochemically assisted photocatalytic degradation at +0.6 V versus SCE, and 1 h	54	31
PSt-grafted ZnO nanoparticles	[MO] = 20 ppm, [Catalyst] = 1.5 g/L, pH of 7, 30°C, and 5 h	83	32
$ZnFe_2O_4$/TiO_2 photocatalysts	$[TiO_2] = 5$ g/L, $[ZnFe_2O_4] = 1.5\%$, [MO] = 25 mg/L, 4 h	84	33
Natural rutile sample containing substituting metal ions as V^{5+} and Fe^{3+}	[rutile] = 1 g/L, [MO] = 11.307 mg/L, $[H_2O_2] = 3.8$ m*M*, $[V_2O_5] = 1.22$ wt %, [FeO] = 0.39 wt %, pH of 3, and 1 h	61	34
$H_4SiW_{12}O_{40}$/PVA/PMMA composite nanofiber membrane	$[H_4SiW_{12}O_{40}] = 1$ g/L, [MO] = 10 mg/L, pH of 1, and 0.5 h	95	This study

SCE, Saturated Calomel Electrode; PSt, Polystyrene.

this nanofiber membrane. The photocatalytic activity of the composite nanofiber membranes decreased with increasing PMMA. This was mainly due to the different morphologies of the composite nanofibers when the PMMA content increased. The increasing amount of beads led to lower specific surface areas and relatively rough surfaces of the nanofibers; it resulted in less exposure of photocatalyst and poor water tolerance of the composite nanofiber membranes.

The linear simulation kinetic curves of MO photocatalytic degradation over different $H_4SiW_{12}O_{40}$/PVA/PMMA composite nanofiber membranes are displayed in Figure 4(d). The results show that the previous degradation reactions followed a Langmuir–Hinshelwood apparent first-order kinetics model because of the low initial concentrations of the reactants.[27] In this experiment, the initial concentration of MO was 10 mg/L, so the model could be expressed with the following equation:

$$-\ln(C/C_0) = k_{app}t \quad (1)$$

where C_0 is the initial concentration of the reactant (mg/L), C is the concentration of the reactant at time t (mg/L), t is the UV-light illumination time, and k_{app} is the apparent first-order rate constant (min^{-1}).[28] The determined k_{app} values were 0.149, 0.089, and 0.065 for the composite nanofiber membranes in which the PMMA/PVA ratios were 1:2, 1:1, and 2:1, respectively. It was clear that the membrane in which the PMMA/PVA ratio was 1:2 showed a better performance than the other two samples; this further confirmed the conclusions stated previously.

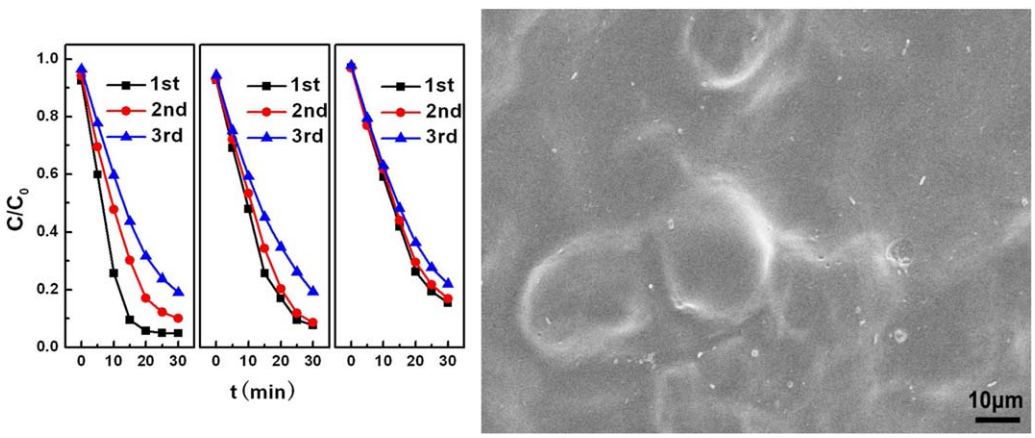

Figure 5. (a) Photodegradation of MO by the $H_4SiW_{12}O_{40}$/PVA/PMMA composite nanofiber membranes with different mass ratios of PMMA to PVA (1:2, 1:1, and 2:1) after a three-cycle experiment and (b) SEM image of the $H_4SiW_{12}O_{40}$/PVA composite nanofiber membrane after the first photocatalytic process. [Color figure can be viewed in the online issue, which is available at wileyonlinelibrary.com.]

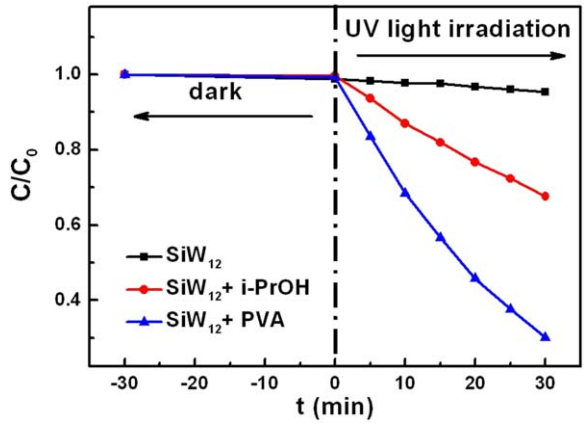

Figure 6. Photodegradation of MO by $H_4SiW_{12}O_{40}$ (powder, 0.05 g), $H_4SiW_{12}O_{40}$ (powder) plus i-PrOH (1.7 mmol), and $H_4SiW_{12}O_{40}$ (powder) plus PVA (a mole of —OH was 1.7 mmol). [Color figure can be viewed in the online issue, which is available at wileyonlinelibrary.com.]

The photocatalytic efficiency in the degradation of MO with other materials reported in previous studies was compared with that found in this study, as shown in Table I. It was clear that the as-prepared $H_4SiW_{12}O_{40}$/PVA/PMMA composite nanofiber membranes exhibited superior photocatalytic activity.

Reusability. Cycling uses and maintaining a high photocatalytic activity is a critical issue for long-term use in practical applications of the catalyst. In view of this, two factors needed to be considered: one was the ease with which the catalyst could be separated from reaction system, and the other was the stability of the catalyst to maintain its high activity over time.[35] In this study, $H_4SiW_{12}O_{40}$/PVA/PMMA composite nanofiber membranes could be directly separated from the aqueous MO solution without any separation process. To examine the stability of the composite nanofiber membranes, the membranes were used three times. As shown in Figure 5(a), we observed that the composite nanofiber membranes presented a small reduction in photocatalytic activity after a three-cycle experiment. This was closely associated with the presence of PMMA and led to a decrease in the hydrophilicity of the composite nanofiber membranes. The osmosis of the aqueous solution into the composite nanofibers was inhibited efficiently, so the stability of the composite nanofiber membranes was improved. On the contrary, there was macroscopic breakage for the $H_4SiW_{12}O_{40}$/PVA composite nanofiber membrane in the first photocatalytic process. Most of the composite nanofiber membrane dissolved in the aqueous solution, and the structure and porosity of the $H_4SiW_{12}O_{40}$/PVA electrospun nanofibers disappeared completely [Figure 5(b)], so the $H_4SiW_{12}O_{40}$/PVA composite nanofiber membrane nearly could not be reused.

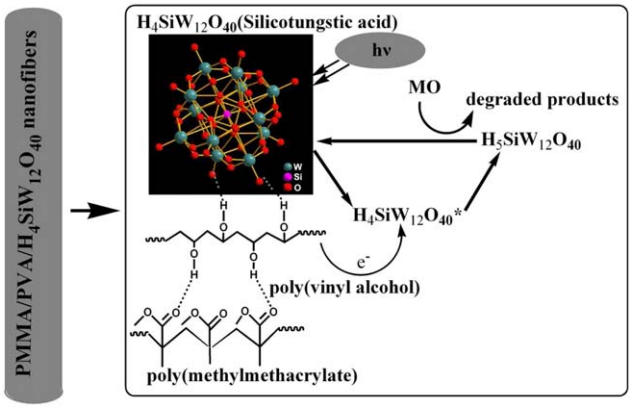

Figure 7. Photocatalytic mechanism of the $H_4SiW_{12}O_{40}$/PVA/PMMA composite nanofiber membrane. [Color figure can be viewed in the online issue, which is available at wileyonlinelibrary.com.]

Possible Photocatalytic Mechanism. The photooxidative degradation of azo dyes by POM has been reported in earlier publications. The process involved the excitation of POM by near UV–vis light; this led to the charge transfer from an O^{2-} ion to a W^{6+} ion at the W—O—W bonds and the formation of a strongly oxidizing excited state of POM (POM*) or POM ($h^+ + e^-$). The photooxidation of the azo dye was performed via the reaction through OH radicals or the direct reaction of the excited POM with the substrate.[19,36] This photocatalytic processes was analogous to TiO_2.[37–39] However, studies[40–43] have proven that in the presence of alcohol [methanol, ethanol, and isopropyl alcohol (i-PrOH)] as a sacrificial electron donor, the whole process is driven by the reductive pathway with a much faster degradation rate. In contrast, the effect of i-PrOH and PVA on the photocatalytic activity of $H_4SiW_{12}O_{40}$ powder was carried out. As shown in Figure (6 and 4).6, 32.4, and 69.9% degradations of MO were observed after 30 min of irradiation in the $H_4SiW_{12}O_{40}$ powder, $H_4SiW_{12}O_{40}$ (powder) plus i-PrOH, and $H_4SiW_{12}O_{40}$ (powder) plus PVA redox systems, respectively. The experimental findings suggest that both i-PrOH and PVA enhanced the photocatalytic activity of $H_4SiW_{12}O_{40}$, whereas PVA exhibited more efficiency. According to the literature[3] and the experimental results, the possible mechanistic scheme for the degradation of MO on the $H_4SiW_{12}O_{40}$/PVA/PMMA composite nanofiber membranes under UV irradiation can be summarized as follows:

$$H_4SiW_{12}O_{40} + h\nu \longleftrightarrow H_4SiW_{12}O_{40}* \quad (1)$$

$$H_4SiW_{12}O_{40}* + \text{PVA} \rightarrow H_5SiW_{12}O_{40} + \text{Oxidation products} \quad (2)$$

$$H_5SiW_{12}O_{40} + \text{MO} \rightarrow H_4SiW_{12}O_{40} + \text{Reduction products} \quad (3)$$

$H_4SiW_{12}O_{40}$ absorbs light and mediates the electron transfer from PVA, the sacrificial donor, to MO. Equations (1) and (2) describe the photocatalytic oxidation of PVA and the

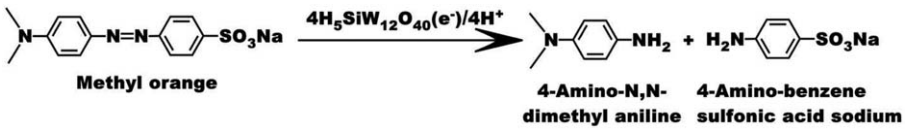

Scheme 1. Degradation pattern of MO in the presence of the composite nanofiber membrane.

simultaneous formation of $H_5SiW_{12}O_{40}$ ($H_5SiW_{12}O_{40}$ is the chemical formula of Silicotungstic acid with one more electron, in which tungsten is pentavalent), whereas eq. (3) describes the fast reoxidation of $H_5SiW_{12}O_{40}$ in the presence of MO molecules (Figure 7). PVA, like other alcohols that possess readily abstractable α-H atoms, may play an important role in the rate of $H_5SiW_{12}O_{40}$ production and, hence, in the degradation rate. The reductive cleavage of the —N=N— bond in the case of MO dye requires four electrons and four H^+ to be completely reduced; this results in the formation of 4-amino-*N*,*N*-dimethyl aniline and 4-aminobenzene sulfonic acid sodium (Scheme 1).

CONCLUSIONS

In summary, $H_4SiW_{12}O_{40}$/PVA/PMMA composite nanofiber membranes were prepared by an electrospinning technique. The IR and XPS results suggest that $H_4SiW_{12}O_{40}$ with an intact Keggin structure existed in the composite nanofiber membrane. The investigation of the photocatalytic ability indicated that the composite nanofiber membranes displayed enhanced photocatalytic activity in the decomposition of MO; this may have been due to the large specific surface area of the nanofiber membranes, low hydrophilicity of the membrane, and photoreduction mechanism. More important, the composite nanofiber membranes were stable in aqueous solution, so they could be easily separated and reused without any separation process. In view of this, the $H_4SiW_{12}O_{40}$/PVA/PMMA composite nanofiber membranes exhibited the potential for practical applications in the elimination of organic pollutants from wastewater.

ACKNOWLEDGMENTS

This work was supported by the National Natural Science Foundation of China (contract grant numbers 51172062 and 51472074), the Scientific Research Foundation for Colleges and Universities of Hebei Province (grant for project QN2014051), the Hundred Talents Program of Hebei Province of China (contract grant number E2012100005), and the Engagement Fund of North China University of Science and Technology (contract grant number GP201517), to which the authors express their grateful appreciation.

REFERENCES

1. Yamase, T. *Catal. Surveys Asia* **2003**, *7*, 203.
2. Li, T.; Gao, S.; Li, F.; Cao, R. *J. Colloid Interface Sci.* **2009**, *338*, 500.
3. Troupis, A.; Triantis, T. M.; Gkika, E.; Hiskia, A.; Papaconstantinou, E. *Appl. Catal. B* **2009**, *86*, 98.
4. Zhou, W.; Cao, M.; Li, N.; Su, S.; Zhao, X.; Wang, J.; Li, X.; Hu, C. *Mater. Res. Bull.* **2013**, *48*, 2308.
5. Molinari, A.; Amadelli, R.; Carassiti, V.; Maldotti, A. *Eur. J. Inorg. Chem.* **2000**, *2000*, 91.
6. Bonchio, M.; Carraro, M.; Scorrano, G.; Fontananova, E.; Drioli, E. *Adv. Synth. Catal.* **2003**, *345*, 1119.
7. Yue, B.; Zhou, Y.; Xu, J.; Wu, Z.; Zhang, X.; Zou, Y.; Jin, S. *Environ. Sci. Technol.* **2002**, *36*, 1325.
8. Ozer, R. R.; Ferry, J. L. *J. Phys. Chem. B* **2002**, *106*, 4336.
9. Molinari, A.; Amadelli, R.; Andreotti, L.; Maldotti, A. *J. Chem. Soc. Dalton Trans.* **1999**, *8*, 1203.
10. Verhoef, M. J.; Kooyman, P. J.; Peters, J. A.; van Bekkum, H. *Micropor. Mesopor. Mater.* **1999**, *27*, 365.
11. Gao, S.; Pan, D.; Cao, R. *J. Colloid Interface Sci.* **2011**, *358*, 593.
12. Zhang, Z.; Shao, C.; Zhang, L.; Li, X.; Liu, Y. *J. Colloid Interface Sci.* **2010**, *351*, 57.
13. Li, J.; Cheng, Z.; Liu, M.; Zhang, M.; Hu, M.; Zhang, L.; Jiang, H.; Li, J. *J. Appl. Polym. Sci.* **2015**, 132.
14. Buchko, C. J.; Chen, L. C.; Shen, Y.; Martin, D. C. *Polymer* **1999**, *40*, 7397.
15. Ye, S.; Zhang, D.; Liu, H.; Zhou, J. *J. Appl. Polym. Sci.* **2011**, *121*, 1757.
16. Saeed, K.; Haider, S.; Oh, T.-J.; Park, S.-Y. *J. Membr. Sci.* **2008**, *322*, 400.
17. Guo, Z.; Shao, C.; Mu, J.; Zhang, M.; Zhang, Z.; Zhang, P.; Chen, B.; Liu, Y. *Catal. Commun.* **2011**, *12*, 880.
18. Kozhevnikov, I. V. *Chem. Rev.* **1998**, *98*, 171.
19. Guo, Y.; Hu, C. *J. Mol. Catal. A* **2007**, *262*, 136.
20. Sui, C.; Li, C.; Guo, X.; Cheng, T.; Gao, Y.; Zhou, G.; Gong, J.; Du, J. *Appl. Surf. Sci.* **2012**, *258*, 7105.
21. Feng, L.; Song, Y.; Zhai, J.; Liu, B.; Xu, J.; Jiang, L.; Zhu, D. *Angew. Chem. Int. Ed.* **2003**, *42*, 800.
22. Naebe, M.; Lin, T.; Staiger, M. P.; Dai, L.; Wang, X. *Nanotechnology* **2008**, *19*, 305702.
23. Sun, T.; Feng, L.; Gao, X.; Jiang, L. *Acc. Chem. Res.* **2005**, *38*, 644.
24. Feng, C.; Shang, H. *Chem. Res. Chin. Univ.* **2012**, *28*, 366.
25. Berry, F. J.; Derrick, G. R.; Marco, J. F.; Mortimer, M. *Mater. Chem. Phys.* **2009**, *114*, 1000.
26. Newman, A. D.; Brown, D. R.; Siril, P.; Lee, A. F.; Wilson, K. *Phys. Chem. Chem. Phys.* **2006**, *8*, 2893.
27. Turchi, C. S.; Ollis, D. F. *J. Catal.* **1990**, *122*, 178.
28. Lee, M. S.; Park, S. S.; Lee, G.-D.; Ju, C.-S.; Hong, S.-S. *Catal. Today* **2005**, *101*, 283.
29. Arabatzis, I. M.; Stergiopoulos, T.; Bernard, M. C.; Labou, D.; Neophytides, S. G.; Falaras, P. *Appl. Catal. B* **2003**, *42*, 187.
30. Parida, K. M.; Sahu, N.; Biswal, N. R.; Naik, B.; Pradhan, A. C. *J. Colloid Interface Sci.* **2008**, *318*, 231.
31. Sohn, Y. S.; Smith, Y. R.; Misra, M.; Subramanian, V. *Appl. Catal. B* **2008**, *84*, 372.
32. Hong, R. Y.; Li, J. H.; Chen, L. L.; Liu, D. Q.; Li, H. Z.; Zheng, Y.; Ding, J. *Powder Technol.* **2009**, *189*, 426.
33. Cheng, P.; Deng, C.; Gu, M.; Shangguan, W. *J. Mater. Sci.* **2007**, *42*, 9239.
34. Lu, A.; Li, Y.; Lv, M.; Wang, C.; Yang, L.; Liu, J.; Wang, Y.; Wong, K.-H.; Wong, P.-K. *Solar Energy Mater. Solar Cells* **2007**, *91*, 1849.
35. Zhang, P.; Shao, C.; Li, X.; Zhang, M.; Zhang, X.; Sun, Y.; Liu, Y. *J. Hazard. Mater.* **2012**, *237*, 331.
36. Hiskia, A.; Mylonas, A.; Papaconstantinou, E. *Chem. Soc. Rev.* **2001**, *30*, 62.

37. Velegraki, T.; Poulios, I.; Charalabaki, M.; Kalogerakis, N.; Samaras, P.; Mantzavinos, D. *Appl. Catal. B* **2006**, *62*, 159.

38. Jyothi, M. S.; Padaki, M.; Geetha Balakrishna, R.; Krishna Pai, R. *J. Mater. Res.* **2014**, *29*, 1537.

39. Nayak, V.; Jyothi, M. S.; Balakrishna, R. G.; Padaki, M.; Ismail, A. F. *ChemistryOpen* **2015**, *4*, 278.

40. Arslan-Alaton, I. *Dyes Pigments* **2004**, *60*, 167.

41. Arslan-Alaton, I.; Ferry, J. L. *J. Photochem. Photobiol. A* **2002**, *152*, 175.

42. Troupis, A.; Gkika, E.; Triantis, T.; Hiskia, A.; Papaconstantinou, E. *J. Photochem. Photobiol. A* **2007**, *188*, 272.

43. Wang, Y.; Lu, K.; Feng, C. *J. Rare Earths* **2013**, *31*, 360.